

Blending in Gravitational Microlensing Experiments: Source Confusion And Related Systematics

Martin C. Smith¹, Przemysław Woźniak², Shude Mao³, Takahiro Sumi^{4,5} \star

¹*Kapteyn Astronomical Institute, University of Groningen, P.O. Box 800, 9700 AV Groningen, Netherlands*

²*Los Alamos National Laboratory, MS-D436, Los Alamos, NM 87545, USA*

³*Univ. of Manchester, Jodrell Bank Observatory, Macclesfield, Cheshire SK11 9DL, UK*

⁴*Princeton University Observatory, Princeton, NJ 08544-1001, USA*

⁵*Solar Terrestrial Environment Laboratory, Nagoya University, Nagoya, Aichi 464-8601, Japan*

Accepted Received; in original form

ABSTRACT

Gravitational microlensing surveys target very dense stellar fields in the local group. As a consequence the microlensed source stars are often blended with nearby unresolved stars. The presence of ‘blending’ is a cause of major uncertainty when determining the lensing properties of events towards the Galactic centre. After demonstrating empirical cases of blending we utilize Monte Carlo simulations to probe the effects of blending. We generate artificial microlensing events using an *HST* luminosity function convolved to typical ground-based seeing, adopting a range of values for the stellar density and seeing. Microlensing light curves are generated using typical sampling and errors from the second phase of the Optical Gravitational Lensing Experiment. We find that a significant fraction of bright events are blended, contrary to the oft-quoted assumption that bright events should be free from blending. We probe the effect that this erroneous assumption has on both the observed event timescale distribution and the optical depth, using realistic detection criteria relevant to the different surveys. Importantly, under this assumption the latter quantity appears to be reasonably unaffected across our adopted values for seeing and density. The timescale distribution is however biased towards smaller values, even for the least dense fields. The dominant source of blending is from lensing of faint source stars, rather than lensing of bright source stars blended with nearby fainter stars. We also explore other issues, such as the centroid motion of blended events and the phenomena of ‘negative’ blending. Furthermore, we briefly note that blending can affect the determination of the centre of the red clump giant region from an observed luminosity function. This has implications for a variety of studies, for example mapping extinction towards the bulge and attempts to constrain the parameters of the Galactic bar through red clump giant number counts. We conclude that blending will be of crucial importance for future microlensing experiments if they wish to determine the optical depth to within 10 per cent or better.

Key words: gravitational lensing - Galaxy: bulge - Galaxy: centre

1 INTRODUCTION

Gravitational microlensing is maturing into an important astrophysical technique with diverse applications to Galactic astronomy, such as probing the dark matter content of the inner Galaxy (see, e.g., the following review articles: Paczyński 1996; Mao 1999; Evans 2003). Thousands of microlensing events have been discovered. The vast majority of these are towards the Galactic centre and many were

identified in real-time, for example by the OGLE¹ (Udalski 2004) or MOA² (Bond et al. 2001) alert systems. The microlensing probability (known as the optical depth, τ) towards the Galactic centre probes the mass distribution along the line of sight. The earliest determinations yield optical depths (Udalski et al. 1994a; Alcock et al. 1997a; Alcock et al. 2000) that are significantly higher than the theoretical predictions (e.g., Zhao & Mao 1996; Binney, Bissantz & Gerhard 2000; Evans & Belokurov 2002; Han & Gould 2003). More recent determinations yield both lower values (Popowski et

\star e-mail: msmith@astro.rug.nl; woźniak@nis.lanl.gov; smao@jb.man.ac.uk; sumi@stelab.nagoya-u.ac.jp

¹ <http://www.astrouw.edu.pl/~ogle/ogle3/ews/ews.html>

² <http://www.massey.ac.nz/~iabond/alert/alert.html>

al. 2005; Hamadache et al. 2006; Sumi et al. 2006) and higher values (Sumi et al. 2003), although these determinations are based on relatively small samples of microlensing events. It is important to note that there appears to be a clear distinction between the measured values of τ for the two commonly-used techniques: higher values of τ are found for determinations carried out using all stars (e.g. Alcock et al. 2000; Sumi et al. 2003), whereas lower values are found when (as advocated by Gould [1995]) only bright stars are used in the analysis (e.g. Popowski et al. 2005; Hamadache et al. 2006; Sumi et al. 2006).

It was realised quite early on (e.g. Udalski et al. 1994a; Alcock et al. 1997b) that blending is a major uncertainty in the determination of τ . Blending occurs naturally because microlensing surveys are conducted in crowded stellar fields and, with typical ground-based seeing, other stars can blend into the seeing disk of the lensed star (see, for example Han 1999 and references therein). This affects the number of potential lensed sources and also introduces uncertainties into the fitted event parameters (e.g. Woźniak & Paczyński 1997; Han 1999). Importantly, it was proposed that the aforementioned discrepancy between the τ measurements from all stars compared to bright stars could be explained by blending.

Clearly the ideal way to understand this blending issue is with high resolution *Hubble Space Telescope* (*HST*) images (Han 1997), which can be used to resolve any nearby blends that may be present. This technique was adopted by Alcock et al. (2001a) in their analysis of a set of microlensing events towards the Large Magellanic Cloud. However, in general this method is limited due to the restrictions on the availability of *HST* observing time. Therefore, in the absence of high resolution images for each event, the next best approach is to undertake Monte Carlo simulations at the pixel level. Mock images can be generated based on deep *HST* luminosity functions of the Galactic bulge. Unfortunately, since such luminosity functions are currently only available for a very limited number of lines of sight (e.g. Holtzman et al. 1998), one must extrapolate their behaviour for the various bulge fields observed by microlensing collaborations. Artificial microlensing stars can be injected into mock images and then convolved into ground-based seeing. It is then possible to investigate the efficiency of recovering microlensing events, i.e. the detection efficiency (see, for example, Alcock et al. 2000). In order to simplify the analysis many microlensing studies concentrate on bright stars, working under the assumption that bright stars suffer negligible blending. However, the reliability of this assumption has recently been called into question (see Section 2). As a result, proper consideration must be given to blending, even when one considers microlensing of bright stars.

Monte Carlo simulations of blending have already been carried out by various groups, mostly concentrating on the effect to the recovered microlensing optical depth. Recent studies include Popowski et al. (2005) and Hamadache et al. (2006), both of which argue that the recovery of the optical depth should not be significantly biased by the presence of blending in bright events. The analysis presented in this paper builds upon another such work (Sumi et al. 2005), which showed that a simulated sample of bright microlensing events still contains many heavily blended events. We extend the work of Sumi et al. (2005) by generalising the analysis to fields with varying stellar density under different seeing conditions. By doing this we aim to make broader conclusions that go beyond any experiment-specific analysis.

The outline of the paper is as follows, in Section 2 we briefly discuss some of the observational evidence that exists to suggest that bright microlensing might not avoid the problem of blending. The remaining sections deal with Monte Carlo simulations that we

have undertaken in order to investigate this phenomenon: Section 3 describes the method; Sections 4 & 5 present the results of our simulations including the resulting distributions of event parameters; Section 6 investigates whether the assumption that bright events are unblended can bias the measured value for the optical depth; and Section 7 discusses the expected distributions of centroid motions. We conclude with Section 8, where we discuss the implications of our findings.

2 OBSERVATIONAL EVIDENCE OF BLENDING IN BRIGHT EVENTS

Although it is often assumed that in general bright events are not affected by blending, there is observational evidence to show that this is not always a safe assumption. In the following section we briefly discuss various different approaches that can be used to test this hypothesis for observed events using ground-based data. We provide a number of examples of bright events that exhibit significant blending.

Throughout this section and the rest of the paper we characterise the blending using the following parameter, f_s , which denotes the ratio of the source flux to the total baseline flux, i.e.

$$f_s = \frac{F_{\text{source}}}{F_{\text{baseline}}}. \quad (1)$$

Therefore, $f_s = 1$ for the case of no blending, while $f_s \rightarrow 0$ for heavily blended events.

2.1 General model fitting

Numerous catalogues of gravitational microlensing events have been published towards the Galactic bulge. Many of these contain bright events that model fitting has suggested are blended, such as the MACHO catalogue of Alcock et al. (2000). This catalogue contains a subset of 37 events that are described as ‘classical lensing’ from which one can determine the fitted blending parameter. Four of these events are both bright ($V < 18$) and heavily blended ($f_s < 0.2$): namely 95-BLG-d19, 97-BLG-d13, 97-BLG-24, 97-BLG-37. All of these four events have reasonably well constrained values of the blending parameter. Popowski et al. (2005) also noted that based on light curve fitting they cannot exclude the possibility of significant blending for some events in their clump-giant sample.

Further examples can be found in the catalogue of clump-giant EROS events published by Afonso et al. (2003), in which two of 16 bright events were found to display clear blending signatures (EROS-BLG-31 and EROS-BLG-12). In contrast, a more recent analysis of the EROS data (Hamadache et al. 2006) finds only five of 120 clump giant events appear to exhibit strong blending, although they acknowledge that their paucity of blended events could be due to the limited photometric precision of the EROS experiment.

In their analysis of the OGLE-II catalogue of bright events, Sumi et al. (2006) found that blending was significant for a number of their events. According to their best-fitting models, 38 per cent of these bright events were actually due to lensing of much fainter sources.

2.2 Centroid motion

Another way to assess the influence of blending is to investigate the motion of the light centroid during the event. The light cen-

centroid is determined by the light from the lens, the lensed source, and/or blended stars along the line of sight. Therefore, during microlensing, the light centroid must shift towards the lensed star as it brightens (e.g., Alard, Mao & Guibert 1995; Goldberg 1998). If the lens dominates the blend, the centroid shift is difficult to detect because the lens and the lensed source are aligned to within milliarcseconds (\sim angular Einstein radius). However, if the blending is mostly due to other blended stars, then the centroid shift may be detectable, even in ground-based observations.

Another similar approach is to measure the offset between the lensed source and the centroid of the light at baseline (Han 2000); this approach can be used when dealing with Difference Image Analysis (DIA), since in this case the location of the lensed source can be measured to high accuracy. It is also possible to try and locate the blend by removing the light of the lensed source using image subtraction (Gould & An 2002; Smith et al. 2002).

These techniques have been applied in various works. The offset between the lensed source and the baseline centroid has been routinely measured for various microlensing catalogues (e.g. Alcock et al. 1999; Alcock et al. 2000; Woźniak et al. 2001). In many cases there are a significant fraction of events with offsets of 1 arcsec or greater.

The first such detections of centroid motions have been presented in Alard, Mao & Guibert (1995) and Goldberg & Woźniak (1998). To further test this effect we have examined the centroid motion for a sample of red clump giant microlensing events from OGLE-II (Sumi et al. 2005). In order to constrain the offset between the lensed star and the blend, we fit the light curve and the centroid positions simultaneously. Fig. 1 shows the event with the most significant centroid shift (sc37–556534), which has a very bright baseline magnitude ($I = 15.9$ mag). As expected, the centroid location is a strong function of the magnitude (magnification). The offset (in pixels, where 1 pixel corresponds to 0.417 arcsec) between the lensed star and the blend is $\Delta x \approx 0.61$, $\Delta y \approx -1.04$. This centroid shift clearly demonstrates that blending can be important for bright microlensing events.

2.3 Binary lens blending

Blending can be inferred not only for single microlensing events, but also for binary microlensing events. In fact, the first (Udalski et al. 1994b) and second (Alard, Mao & Guibert 1995) binary lens events both show significant blending. Detailed studies of binary lenses in OGLE-II (Jaroszyński 2002) and OGLE-III data (Jaroszyński et al. 2004) show convincingly that blending in binary lenses is widespread; they find that the fractions of bright events (observed $I < 18$) with fitted parameter $f_s < 0.5$ are 3/5 and 4/7 for OGLE-II and OGLE-III, respectively. The most spectacular example is sc5_6650 from OGLE-II, for which the lensed source is inferred to contribute only 1 per cent of the total light even though the composite is very bright with a baseline magnitude $I = 16.18$.

Binary light curves are very diverse and, as a result, poorly sampled ones can often be fitted with multiple models (e.g., Mao & Di Stefano 1995; Albrow et al. 1999; Dominik 1999; Gaudi & Han 2004). This problem often renders the f_s determination somewhat uncertain. However, for binary events that undergo a caustic crossing, a limit on the blending can often be inferred without any detailed modelling. These binary events exhibit ‘U’-shaped light curves as the lensed star enters and then exits from the caustics. The minimum magnification in the plateau must be equal to or exceed 3 (Witt & Mao 1995). If the observed minimum magnification

within this plateau, A_{\min} , is below 3, then the fraction of light contributed by the source must satisfy the inequality,

$$f_s \leq \frac{A_{\min} - 1}{2}, \quad A_{\min} \leq 3. \quad (2)$$

For example, the OGLE-II event sc5_6650 has an observed $A_{\min} \approx 1.04$ and hence we can infer that $f_s \leq 0.02$, which is fully consistent with the blending parameter ($f_s = 0.01$) obtained by Jaroszyński (2002) from detailed light curve fitting. Kim (2004) presents a more comprehensive analysis of the limits that can be derived for binary events in the OGLE-II and OGLE-III databases; this work shows that 5/7 bright (observed $I < 18$) caustic crossing events have $f_s < 0.5$.

It should be noted that there may be a slight bias in the blending distribution derived from caustic crossing binary events since such events often undergo large amplifications, which increases the probability of observing lensing of faint source stars. However, even given this caveat it is clear that the analysis of binary events can provide a robust model-independent method for investigating blending. As has been shown above, it is evident that for binary lenses (as with single lenses) bright events can be heavily blended.

3 CONSTRUCTION OF A MOCK CATALOGUE OF BLENDED EVENTS

In the remainder of this paper we undertake Monte Carlo simulations in order to investigate the effect of blending for simulated bulge fields with varying seeing and densities. In this section we discuss the construction of our catalogue of mock microlensing events.

We first construct artificial images for 9 simulated fields, adopting three different values for the density of stars and three different values for the level of seeing. The densities of our fields are chosen relative to the OGLE-II field sc3, which is centered on $l = 0.11^\circ$, $b = -1.93^\circ$ and has an observed surface density of 151 stars per arcmin² down to a magnitude of $I = 17$. We choose densities of 0.5, 1 and 1.5 times the density of field sc3. The three values of seeing are 2.1, 1.05, 0.7 arcsec. Throughout this paper we designate the field with median seeing and density (i.e. density of field sc3 and seeing of 1.05 arcsec) as our reference field. The details for each of our fields are summarised in Table 1. Similar to the OGLE-II experiment, each field has dimensions 14×57 arcmin² and has pixel size 0.417 arcsec pixel⁻¹. Field sc3 was chosen since it is a very dense stellar field close to the Galactic centre where blending should be most significant. Further details about the OGLE-II experiment can be found in Udalski et al. (2000).

It is helpful to see how the adopted characteristics for our simulated fields compare to the important microlensing bulge surveys. The pixel size and typical seeing values for five of the major microlensing experiments are:

- OGLE-II: 0.42 arcsec pixel size and median seeing ~ 1.3 arcsec (Sumi et al. 2006)
- OGLE-III: 0.26 arcsec pixel size and median seeing ~ 1.3 arcsec
- MACHO: 0.63 arcsec pixel size and median seeing ~ 2.1 arcsec (Popowski et al. 2005)
- EROS-II: 0.6 arcsec pixel size and median seeing ~ 2 arcsec (Palanque-Delabrouille et al. 1998);
- MOA: 0.81 arcsec pixel size and median seeing ~ 2.5 arcsec (Bond et al. 2001).

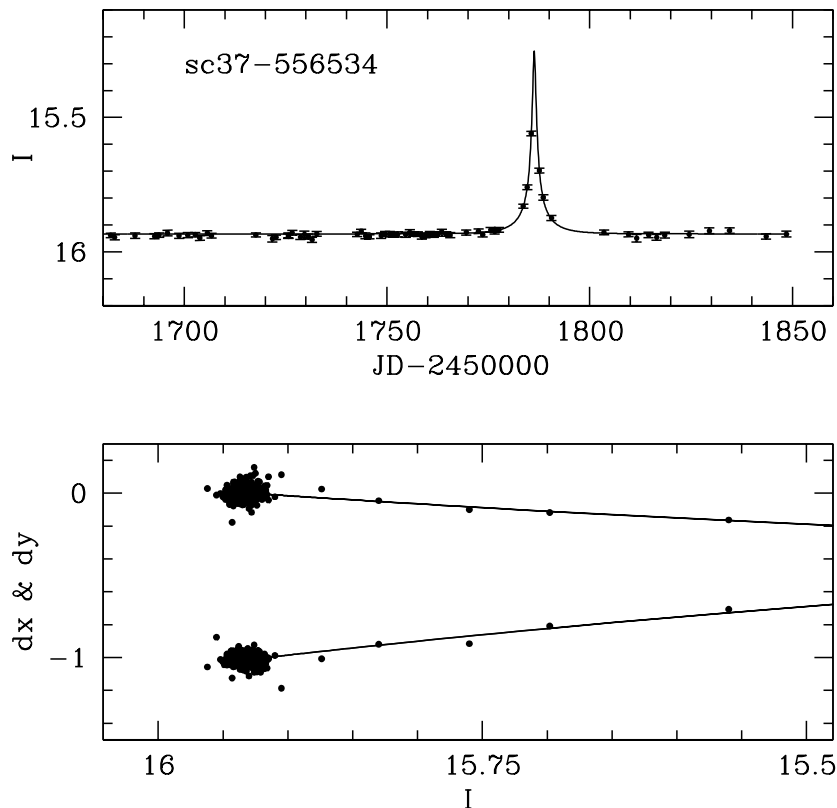


Figure 1. An example of an observed case of centroid motion. The top panel shows the light curve for this event (sc37-556534). The bottom panel shows the corresponding centroid shift for x and y in pixels (1 pixel corresponds to 0.417 arcsec) as a function of I -band magnitude. The solid line indicates the best-fit model. For clarity, the y centroid position has been shifted downward by 1 pixel.

It can be seen that the range of seeing and density for our simulated fields covers practically all bulge surveys, both current and previous. Although our adopted pixel size (corresponding to OGLE-II) is smaller than the non-OGLE experiments listed here, this should not be a dominant effect. It is also worth noting that our choice of medium density, which corresponds to one of the densest OGLE-II fields, is comparable to the densest fields in both MACHO (Popowski et al. 2005) and EROS (Hamadache et al. 2006) optical depth studies.

Our artificial fields are created following the prescription of Sumi et al. (2006); full details of the procedure can be found in section 4.1 of their paper. We populate our field by selecting stars from the *HST* I -band luminosity function of Holtzman et al. (1998). Since the OGLE field sc3 is not coincident with the *HST* field from Holtzman et al. (1998), the *HST* luminosity function must be shifted so as to matches the observed number density of bright stars from the OGLE sc3 field. By combining the OGLE and *HST* data we are also able to constrain the bright end of the luminosity function; this region cannot be well constrained using the *HST* data alone as there are very few bright stars due to saturation and the small field of view. We account for the differential extinction across the field using the extinction maps of Sumi (2004). Note that our simulations are carried out solely with I -band data and do not incorporate any colour information.

Using this luminosity function we populated our field with approximately 10^7 artificial stars down to a magnitude of $I \approx 22$ and then convolved the image to our required level of seeing. Our re-

sulting mock fields are therefore fully synthetic (i.e. artificial stars are not injected into observed fields) and have realistic noise properties, making them effectively indistinguishable from real images. Note that stars are placed randomly in the field and are not placed on a regularly spaced grid.

Given this mock field we then applied the standard OGLE photometry pipeline that is based on DoPHOT (Schechter, Mateo, & Saha 1993) to obtain the ‘observed’ magnitude of the 10^7 artificial stars. From this we can record the ‘input’ magnitude of the artificial star (I_{in}) and the resulting ‘output’ magnitude as measured by DoPHOT (I_{out}). This ‘output’ magnitude corresponds to the observed baseline for a star. Ideally, we should find that $I_{\text{out}} < I_{\text{in}}$ for all stars, since the ‘output’ magnitude includes many blended stars. However, as will be shown below, this is not true in all cases (see Section 4.2).

Given these ‘input’ and ‘output’ magnitudes we can calculate the the blending fraction, f_S , i.e. the fraction of the baseline flux contributed by the source,

$$f_S = \frac{F_{\text{source}}}{F_{\text{baseline}}} = \frac{F_{\text{source}}}{F_{\text{source}} + F_{\text{blend}}} = 10^{(I_{\text{out}} - I_{\text{in}})/2.5}. \quad (3)$$

However, the resulting blending distribution needs to be corrected for the detection efficiency, since heavily blended events (i.e. $f_S \ll 1$) are less likely to be detected because they require much greater intrinsic magnifications to produce an observed increase in magnitude.

To simulate this effect, we generated a mock catalogue of stan-

dard microlensing light curves using the sampling and photometric properties of the OGLE-II experiment (Udalski et al. 2000): namely, I -band observations taken approximately once every few nights; bulge season typically lasting from mid-February until the end of October; limiting magnitude and saturation are approximately $I \approx 20$ and $I \approx 11.5$, respectively. We choose to generate light curves over a total baseline of three years and assume that each star has an equal probability of being lensed (i.e. we assume all stars belong to the bulge). The generation of these mock catalogues follows the prescription given in Smith et al. (2005) although for the purposes of this paper parallax signatures (Gould 1992) have been neglected. Although it is well known that symmetric parallax signatures can be confused with blending (Smith, Mao & Paczyński 2003), it would be computationally too demanding to generate and fit parallax signatures. In any case, such symmetric parallax events should not be common.

The event timescale is drawn from the model described in Smith et al. (2005) and the impact parameter (in units of the Einstein radius) is chosen uniformly between 0 and 1.5. Note that unless otherwise mentioned, our analysis is based on events with fitted impact parameter less than 1; we generate events with larger impact parameters because when events are fitted with a microlensing model (see Section 5.1.1) the recovered impact parameter can sometimes be underestimated. Photometric errors are assumed to be Gaussian (e.g. Woźniak 2000).

Once this mock catalogue has been produced we apply the selection criteria of Sumi et al. (2005) to simulate the detection efficiency. Essentially, these criteria test for the presence of a constant baseline with one distinct brightening episode.

We divide our mock catalogue into two samples: a full sample of all events with baseline magnitude $I_{\text{out}} < 19$ and a subsample of bright events with $I_{\text{out}} < 17$. This latter subsample of events corresponds to what one would expect to see for a sample of red clump giant microlensing events, for example. We only consider events with $I_{\text{out}} < 19$ since fainter objects are too close to the limiting magnitude of the OGLE-II experiment. These cuts are illustrated in Fig. 2, which shows the observed colour-magnitude diagram for the OGLE-II sc3 field.

4 GENERAL SHAPE OF BLENDING DISTRIBUTION

4.1 General description of blending distribution

The resulting blending distributions for 5 of our simulated fields are shown in Fig. 3. In this figure we show both the full samples of all events ($I_{\text{out}} < 19$) and the bright subsamples of events with baseline magnitude brighter than $I_{\text{out}} < 17$ (see Section 3).

For the full sample of all events, the distributions appear relatively flat between $f_S = 0$ and $f_S = 1$. The most striking feature is the long tail of events with $f_S > 1$, particularly for fields with bad seeing. This feature corresponds to sources that are brighter than the measured baseline (i.e. I_{out}). These so-called ‘negatively blended’ events are discussed in detail in Section 4.2. As expected, there is a significant proportion of heavily blended events; for example, for our reference field (medium density and seeing), 57 per cent have $f_S < 0.5$ and 16 per cent have $f_S < 0.1$. For our different fields the blending distribution follows the anticipated trend, with the better seeing and/or less dense stellar fields exhibiting less blending (see Table 1).

The shape of the blending distribution is quite different for the bright subsample of events. There is a clear ‘u’-shaped distribution

with few events in the region $0.2 < f_S < 0.8$. It has been assumed that bright events may be free from the problem of blending, since any blended star would be too faint to contribute substantially to the total flux. However, it is clear from this figure that a significant proportion of events have $f_S < 0.1$, namely 27 per cent for our reference field. The behaviour for the other fields is very similar, but with fewer heavily blended events for fields with better seeing and/or lower stellar density (see Table 1).

We find that in almost all cases heavily blended events occur in our bright sample when a faint source close to a bright star is lensed. For example, in our reference field we find that for a sample of bright (total baseline magnitude $I_{\text{out}} < 17$), blended events ($f_S < 0.2$), over 99 per cent have source magnitudes fainter than 17th magnitude. There are two competing effects that will determine how frequently such events occur. First, it depends on the luminosity function, i.e. how the number counts rise as the magnitude becomes fainter. If the luminosity function is steep (as is the case for the bright end of the luminosity function), then there are numerous faint stars, which enhances the number of lensed cases with strong blending. Second, in order for strongly blended events to be observable, the intrinsic magnification must be much higher than the nominal threshold ($A > 3/\sqrt{5}$). Given the shape of this f_S distribution, it appears that the assumption that bright events are unblended is not a sound one. We deal with the effects of this assumption in later sections (see Section 5 and 6). As with the full sample of all events there is a fraction of events with negative blending, although for this magnitude range this fraction is smaller (see Section 4.2).

In Fig. 4 and Table 2 we show how the f_S distribution varies as a function of the baseline magnitude (i.e. I_{out}) for our reference field. Although the overall shape of the distribution shows a significant trend across the range of magnitudes, there is no clear trend for the percentage of heavily blended events with $f_S < 0.2$. This fact is interesting in that it is clearly in contradiction with the argument that bright events are free from significant blending.

4.2 Negative blending

Positive blending is obviously induced when the lensed source is blended with other sources that are too close to resolve under ground-based seeing conditions. The case for negative blending is less straightforward. One of the first papers to discuss the issue of negative blended fluxes was Park et al. (2004), which concerned the microlensing event MOA-2003-BLG-37. For this event they obtain a best-fit value of $f_S \approx 1.06$. Further events have been identified by various authors (e.g. Jiang et al. 2004; Poindexter et al. 2005; Sumi et al. 2006).

Fig. 3 shows the extent of the issue for our simulated fields (see also Table 1). Curiously, there are no obvious trends evident in either seeing or density. The only clear effect is that for lowest quality seeing the problem becomes significantly worse, although this could be due to increased photometric noise which is present in fields with such bad seeing. There is also no clear trend between the samples of all events and bright events.

We examined a number of images from our simulations that show negative blending. In many cases we find that it arises when we have another star close to the lensed star, and the DoPHOT photometry program incorrectly partitioned part of the lensed star flux to the nearby blend, yielding a negative blending for the lensed source. Another possibility is a ‘hole’ in the mottled distribution of faint stars that constitutes the background flux. This arises because the DoPHOT program assumes a constant background, while

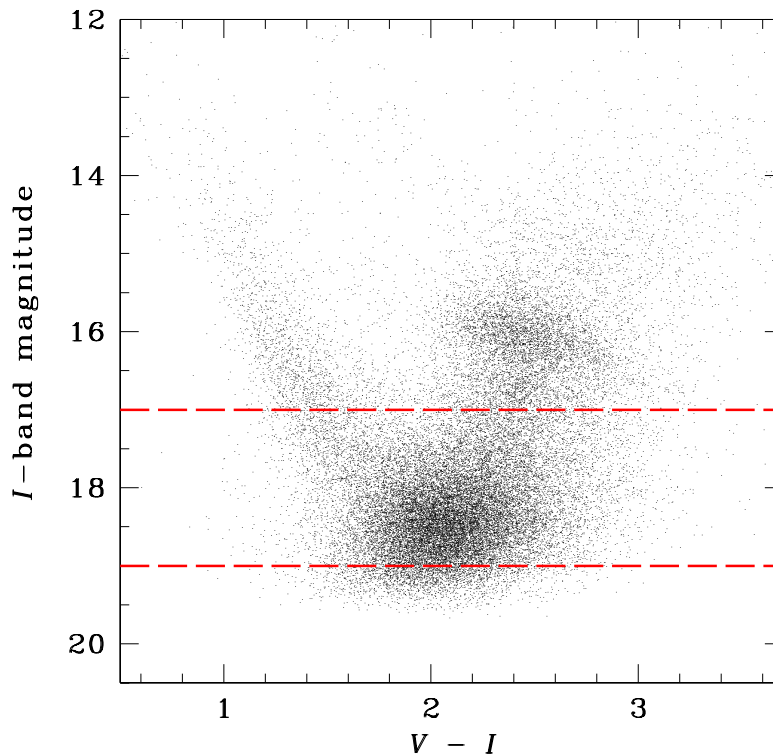


Figure 2. The observed OGLE-II colour-magnitude diagram for field sc3. Note that this is the *observed* field and not a *simulated* field, since we do not include V-band data in our simulations. The horizontal lines show the cuts for all events ($I_{\text{out}} < 19$) and bright events ($I_{\text{out}} < 17$). The latter sample corresponds to a brightness cut similar to that employed for red clump giant microlensing events; for this figure the red clump region is centred around $V - I \approx 2.4$, $I \approx 16$. In reality, a red clump sample would be selected using a cut in colour to remove foreground blue disk stars, but this is not necessary in our case since our simulation contains no colour information and is set up so that all stars belong to the bulge.

in reality the background is contributed by unresolved faint stars which have fluctuations. If the background close to the star is lower than the average background (a ‘hole’), then the DoPHOT program will over-subtract the background, yielding a negative blending for the lensed source. For MOA-2003-BLG-37, the best-fit deblended intrinsic source magnitude $I_0 \approx 14.4$ mag, in order to produce $f_s \approx 1.06$, Park et al. (2004) required a ‘hole’ equivalent to the omission of a $I_0 \approx 17$ mag turn-off star.

To conclude, we are unable to make any definitive statements about the nature of negative blending. We have attempted to show the empirical effects by carrying out analyses that are as close to real surveys as possible. It seems that the causes for negative blending are a combination of those discussed above, namely software issues from deblending and holes in the background, with the additional complication of simple statistical noise.

5 INVESTIGATION OF BLENDING-RELATED BIASES IN THE RECOVERY OF EVENT PARAMETERS

5.1 Fitting of the mock light curves and detection efficiency

5.1.1 Light curve fitting

To investigate the best-fit event parameters we fit each mock light curve with the standard 5-parameter blended microlensing model:

$$I(t) = I_{\text{base}} - 2.5 \log [f_s(A(t) - 1) + 1], \quad (4)$$

where the magnification, $A(t)$, is given by,

$$A(t) = \frac{u(t)^2 + 2}{u(t) \sqrt{u(t)^2 + 4}}, \quad u(t) \equiv \sqrt{u_0^2 + \left(\frac{t - t_0}{t_E}\right)^2}. \quad (5)$$

Here u_0 is the impact parameter in units of the Einstein radius, t_0 is the time of the closest approach (i.e. maximum magnification), and t_E the event timescale. Our parameter t_E corresponds to the Einstein radius crossing time; it should not be confused with the Einstein diameter crossing $\hat{t} = 2t_E$, which is sometimes used by the MACHO collaboration.

The best fit was found by minimizing the χ^2 using the Munit package from the CERN Program Library.³ A full description of the Munit package can be found in the ‘Munit Reference Manual’ (James 1994), which is also available online.

We reject all events for which the timescales are degenerate (i.e. those events for which errors cannot be computed by Munit or events with errors on t_E greater than 30 per cent), since no meaningful parameter values can be extracted from such light curves. This mostly removes low signal-to-noise ratio (S/N) events, although a

³ <http://wwwasdoc.web.cern.ch/wwwasdoc/minuit/>

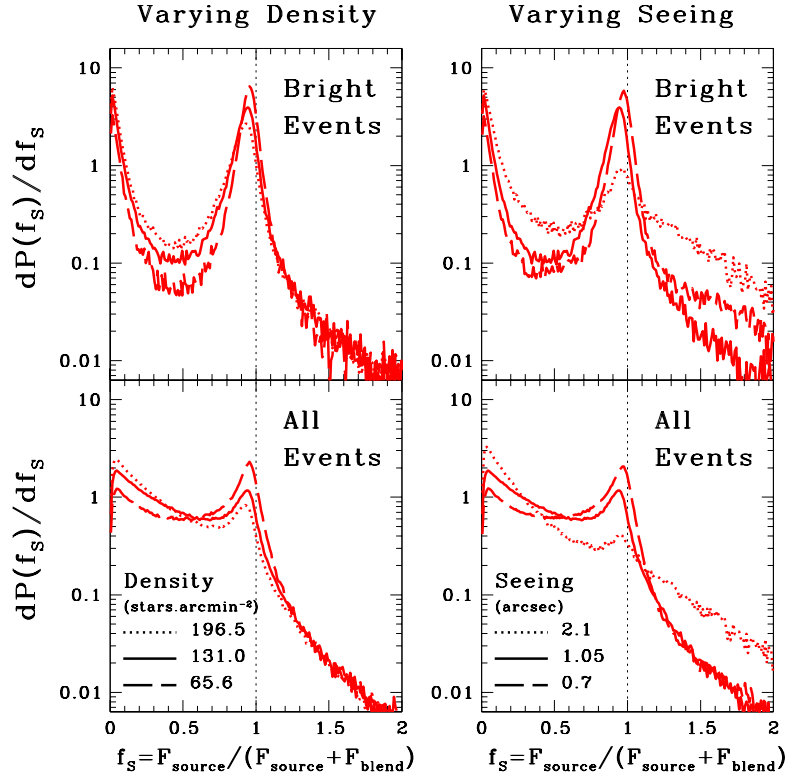


Figure 3. The input (i.e. not fitted) blending distributions for recovered microlensing events in our simulated fields. The upper panel shows the distribution for a bright subset of events ($I_{\text{out}} < 17$), such as red clump giants, and the lower panel shows the distribution for all events (i.e. $I_{\text{out}} < 19$). The left panel shows fields with differing stellar density (dotted/solid/dashed correspond to high/medium/low density) while the right panel shows fields with differing values for the seeing (dotted/solid/dashed corresponds to low/medium/high quality seeing). The vertical line at $f_s = 1$ denotes zero blending, which means that all events to the right of this line exhibit negative blending (see Section 4.2). The small-scale fluctuations in these distributions are due to small number statistics and are not physical.

fraction of these are heavily blended events suffering from the well-known degeneracy between f_s , u_0 and t_E (Woźniak & Paczyński 1997).

Note that it is important that we only deal with events with well-constrained parameters since when we calculate the optical depth for the blended fits (Section 6) we select our bright samples using the fitted source magnitude, which obviously depends on f_s .

5.1.2 Notation convention

In the remainder of this work we adopt the following notation conventions. We use the subscript ‘in’ to denote an ‘input’ property, i.e. the true value of a parameter. For events that have been fitted with a model incorporating blending (i.e. a 5-parameter fit) we use the subscript ‘5p’. Equivalently, for a fit with a model that incorporates no blending (i.e. a 4-parameter fit with $f_s = 1$) we use the subscript ‘4p’. The subscript ‘out’ is sometimes used without an accompanying ‘4p’ or ‘5p’ to denote the fitted parameter in general, i.e. when referring to both 4- and 5-parameter fits.

For the optical depth τ_{in} corresponds to the input τ , as given below by equation (6), and τ_{out} corresponds to the observed value obtained using the best-fitting t_E parameters for the sample of microlensing light curves (equation 7, below).

We also retain the convention for magnitudes described above,

namely that I_{in} refers to the magnitude of a star on the ‘input’ image (i.e. prior to convolving to ground-based seeing) and I_{out} refers to the magnitude of a star on the ‘output’ image (i.e. the resulting magnitude of a star from DoPHOT after the image has been convolved to ground-based seeing). The magnitude I_S denotes the magnitude of the source star, i.e. the star that has been microlensed.

5.1.3 Detection efficiency

The detection efficiency is required when one wishes to compare timescale distributions or calculate optical depths (see Section 6). It is simply the proportion of microlensing events that are recovered as a function of the event timescale, although it can be extended so that it becomes a function of other parameters such as the peak magnification (e.g. Popowski et al. 2005). We only require the efficiency for bright events with $I_{\text{out}} < 17$ mag, since we will not deal with the fainter events in such a rigorous way.

We calculate the detection efficiency separately for our blended and unblended fits. For our unblended fits we are working under the (not necessarily correct) assumption that events brighter than $I_{\text{out}} = 17$ mag are unblended. Therefore for each of our simulated fields we generate a series of mock unblended events using the same method as described in Section 3, where the baseline magnitude of the source is selected from our standard luminosity func-

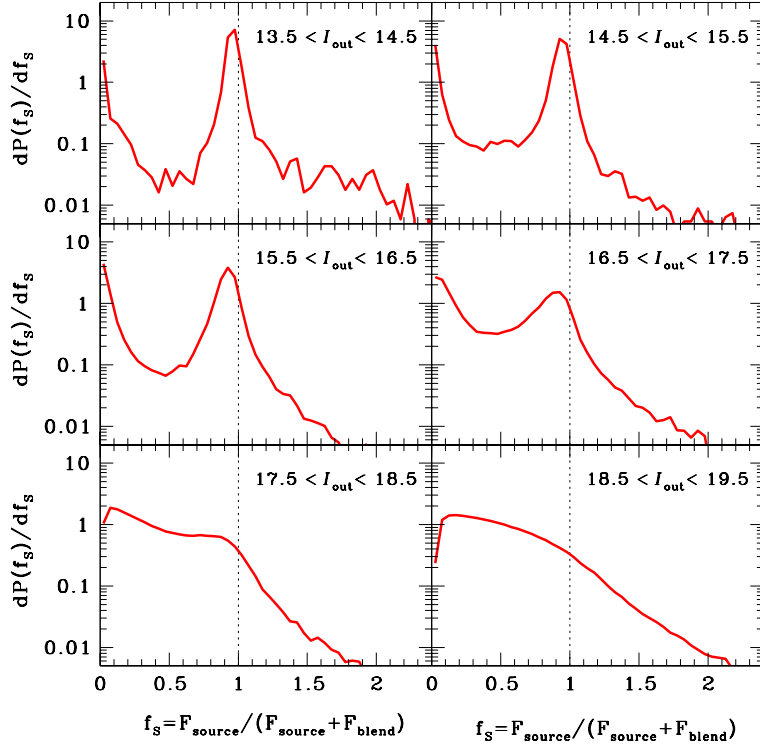


Figure 4. The input (i.e. not fitted) blending distribution for recovered microlensing events for six different output magnitudes, I_{out} . This figure shows the distribution for the simulated field with medium seeing and density. The small-scale fluctuations in these distributions are due to small number statistics and are not physical.

tion. We then apply our 4-parameter fitting routine (Section 5.1.1) and calculate the fraction of events that pass our detection criteria as a function of event timescale. In this case the detection criteria are based on the 4-parameter fits, e.g. $u_{0,4p} < 1$.

The detection efficiency for blended events is very similar to the unblended case, except for these we also incorporate the blended component of the baseline flux into our event generation. This is done using the simulations described in Section 3. We then fit our events with the 5-parameter fit and calculate the proportion of events that pass our detection criteria. Note that the efficiency is much reduced owing to the fact that many of these blended events are degenerate and thus do not pass our selection criteria. It is also important to note that for the blended fits we classify bright events as those with source magnitude brighter than $I_S = 17$ mag, which means that events with $I_{\text{out}} < 17$ can be excluded if they are sufficiently blended.

5.2 The effect of blending for all events

The distributions of the fitted and input event parameters are shown in Fig. 5 for our reference field (medium stellar density and seeing). The bottom panels show the distributions for all events, i.e. $I_{\text{out}} < 19$. For the blending parameter f_S , the fitted distribution matches the input distribution reasonably well except for a slight under-prediction of events with $f_{S,sp}$ just less than one and a slight over-prediction for the number of negatively blended events with

$f_{S,sp} > 1$. Note that this $f_{S,sp}$ distribution differs from that shown in Fig. 3 since this does not include degenerate events from which one cannot gain a reliable estimate on the event parameters. This leads to a reduction in the number of events with small $f_{S,sp}$ owing to the well known degeneracy between f_S , u_0 and t_E (Woźniak & Paczyński 1997). In addition, such heavily blended events often have lower signal-to-noise owing to the fact that these faint source stars require larger amplifications to rise above the detection threshold.

The bottom-right panel shows the fitted timescale distribution for all events ($I_{\text{out}} < 19$). The input timescale distribution ($t_{E,in}$) for the events that pass the microlensing selection criteria almost precisely matches the distribution of fitted timescales ($t_{E,sp}$). The difference in $\langle t_E \rangle$ between these two distributions is less than one per cent. Note that we do not compare the behaviour of the t_E distribution with an actual observed distribution, such as in Alcock et al. (2000), since the nature of the timescale distribution is subject to various uncertainties which we do not wish to consider here. The purpose of this work is solely to show the difference between the fitted and input t_E distributions.

Although in Fig. 5 we only show the distributions for our reference field, the other fields from our simulations exhibit qualitatively similar behaviour.

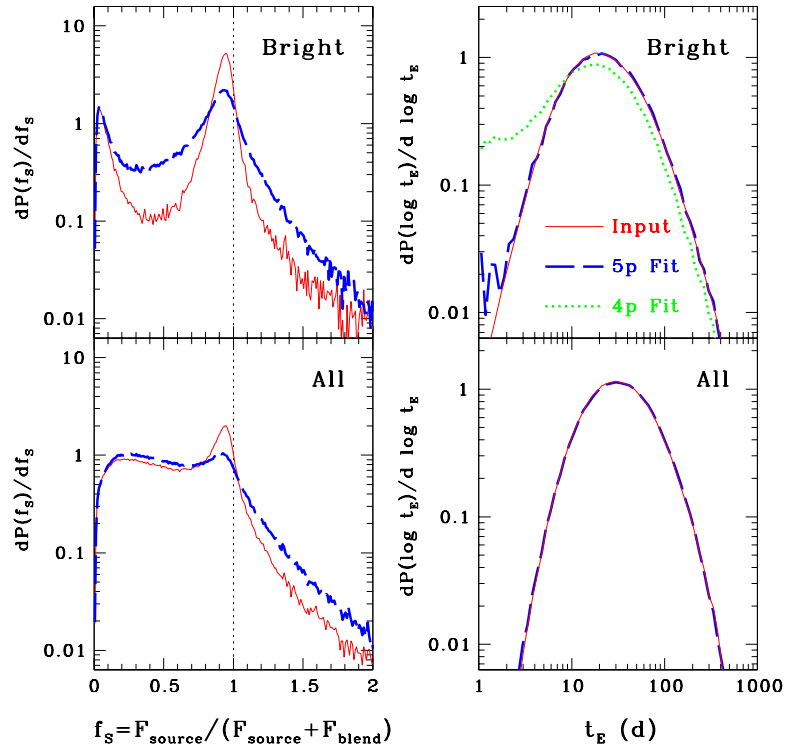


Figure 5. Input and fitted event parameter distributions for the blending fraction (left) the event timescale (right). This figure corresponds to the simulated field with medium stellar density and seeing; the other fields show qualitatively similar behaviour. The solid line represents the input event parameter distribution, the long dashed line represents the 5-parameter fit (i.e. unconstrained blending) and the dotted line represents the 4-parameter fit (i.e. $f_s = 1$). The top panels show the distributions for a subset of bright events ($I_{\text{out}} < 17$), such as red clump giants, and the bottom panels show the distributions for all events (i.e. $I_{\text{out}} < 19$). The fitted timescale distributions in the upper panel are corrected for the detection efficiency and the solid line denotes the underlying timescale distribution; the lower panel simply shows the distributions of input and fitted timescales for the detected events (note that since the two distributions in this panel are almost identical, the two lines are coincident).

5.3 The effect of blending for bright events

The distributions of fitted event parameters for the bright sample of events from our reference field are shown in the upper panels of Fig. 5. As was seen in Fig. 4, the distribution of blending parameter $f_{s,\text{in}}$ shows a ‘u’-shaped distribution for bright events. However, the fitted value of the $f_{s,5p}$ parameter shows a markedly smoother distribution, where an under-prediction in the number of events with $f_{s,5p} \approx 1$ results in an over-prediction of events with $f_{s,5p} \approx 0.5$ and $f_{s,5p} > 1$.

Despite this problem, the distribution of $t_{E,5p}$ matches the input distribution extremely well. In the upper-right panel we show the $t_{E,5p}$ distribution corrected for the microlensing detection efficiency (see Section 5.1.3), along with $t_{E,\text{in}}$ distribution that we used to generate our events. The two distributions are in almost perfect agreement, with the fitted $\langle t_E \rangle$ being recovered to within one per cent.

It is interesting to see what happens to the fitted t_E distribution when we impose the assumption that bright events are unblended. To investigate this we fit our sample of blended mock light curves with a model that enforces no blending (i.e. $f_s = 1$), again correcting for the detection efficiency (Section 5.1.3). The upper-middle panel of Fig. 5 shows the effect of this assumption. There is clearly

a significant tail of short duration events in the distribution of $t_{E,4p}$ that is not present in the input distribution, which is due to the presence of blended events; when blended events are fitted with an unblended model, the resulting timescales are underestimated. However, the fit that incorporates blending does not suffer from this problem. Because of this problem, the $\langle t_{E,4p} \rangle$ is under-estimated by 23 per cent for this field. In the next section we discuss the implications of this assumption on the optical depth.

The qualitative behaviour for the other simulated fields is similar to that shown for our reference field. However, the effect of the assumption that bright events are unblended varies between fields, due to the fact that the level of blending is dependent on the stellar density and seeing. In Figure 6 we show the t_E distribution of the bright sample of events for a selection of fields from our simulations. This figure illustrates that the fields with a greater level of blending (i.e. those with greater density or worse seeing) have more problems reproducing the t_E distribution under the assumptions that bright events are unblended. The corresponding dependence of $\langle t_{E,4p} \rangle$ with density and seeing are tabulated in Table 1 and plotted in Figure 7. Note that while the value of $\langle t_{E,\text{out}} \rangle / \langle t_{E,\text{in}} \rangle$ is not dependent on the seeing or density for the blended fits (for all fields t_E is recovered to within 2 per cent), there is a significant dependence for the unblended fits.

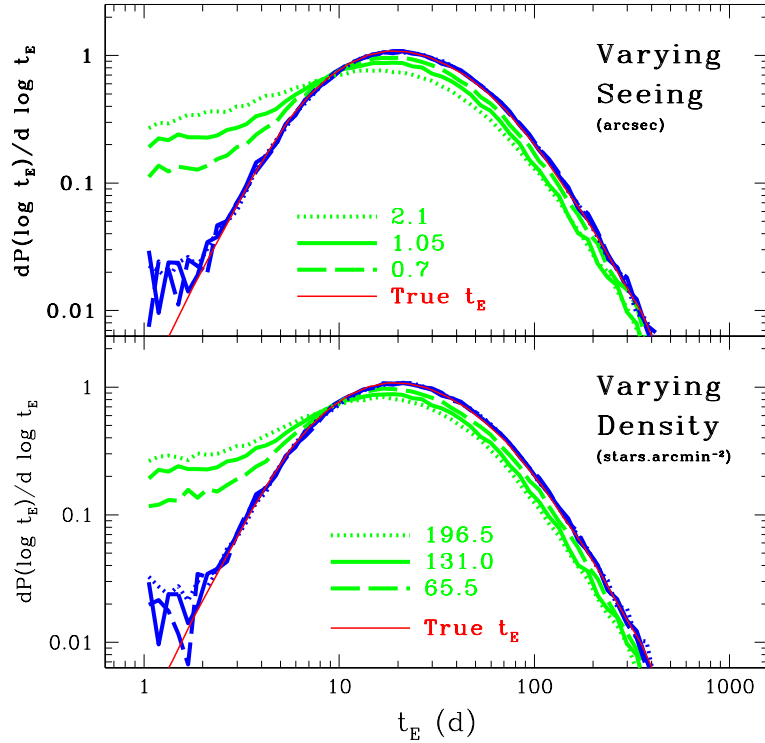


Figure 6. Input and fitted event timescale distributions for various values of density (bottom) and seeing (top). Note that these distributions are corrected for detection efficiency. The thin curves denote the input timescale distribution and the thick curves denote the fitted timescale distributions for the 5-parameter (i.e. unconstrained blending; dark) and 4-parameter (i.e. $f_S = 1$; light) fits. In the bottom panels the dotted/solid/dashed curves correspond to high/medium/low stellar density, while in the top panels the dotted/solid/dashed curves correspond to low/medium/high quality seeing. All curves are only for bright events ($I_{\text{out}} < 17$).

One issue that concerned Hamadache et al. (2006) was the effect of blending from faint stars within the seeing disc of a bright microlensed source (as opposed to the case for which the faint star itself is magnified). We find that for our simulations this is a very weak effect. In our reference field, a sample of bright events with $I_S < 17$ (i.e. source magnitude, not baseline magnitude) contains less than 0.1 per cent that are heavily blended ($f_{S,\text{in}} < 0.2$) and only around 1 per cent with moderate blending ($f_{S,\text{in}} < 0.5$). For these bright event with $I_S < 17$, the error in the recovered $t_{E,4p}$ is negligible; for our reference field the value of $\langle t_{E,4p} \rangle$ is underestimated by only 2.7 per cent. It is clear that the problems caused by blending of bright source stars will be dwarfed by the other, much more prevalent, cause of blending, i.e. microlensing of faint blended source stars below the magnitude cut-off.

6 THE UNCERTAINTY IN THE OPTICAL DEPTH MEASUREMENT DUE TO BLENDING

It is important to quantify whether the assumption that bright microlensing events are unblended leads to any bias in the measurement of the optical depth. As has been shown above, this assumption can lead to a significant error in the value of the mean event timescale. However, it has been argued that this effect cancels out due to an overestimate in the number of events with bright source

stars (e.g. Afonso et al. 2003). It is the misidentification of the true baseline source magnitude that causes this overestimate, since a sample of bright events will be contaminated by fainter source stars that appear brighter than the magnitude cut due to blending. In this section we test the validity of this assumption by taking a sample of bright microlensing events from our simulations and calculating both the input and output optical depth (i.e. both the true value and the measured value as calculated using the conventional methods).

6.1 Method

6.1.1 Input optical depth

The first step in this procedure is to calculate the input optical depth, τ_{in} , for bright source stars (i.e. $I_{\text{in}} < 17$). The optical depth is the probability that a given star is magnified by greater than $3/\sqrt{5}$. This can be estimated for a stellar field by counting the total length of time that any of the bright stars are magnified by greater than $3/\sqrt{5}$, divided by the total number of bright stars and the total duration of the experiment. Since the length of time for which any microlensed star is magnified by greater than $3/\sqrt{5}$ is simply given by $2t_{E,\text{in}}\sqrt{1-u_{0,\text{in}}^2}$, the optical depth for our simulated catalogue can be calculated using the following equation (e.g. Popowski et al. 2005),

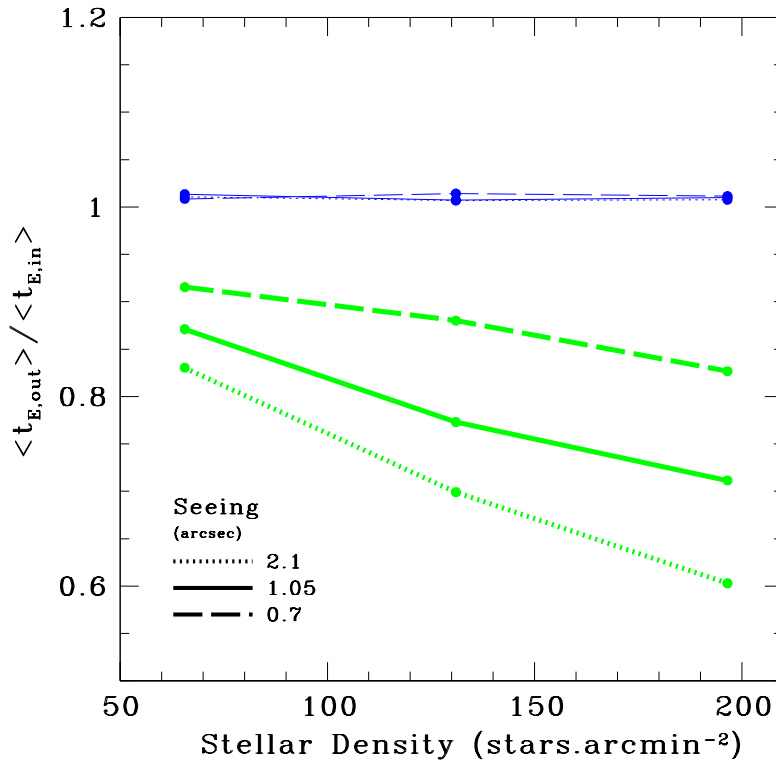


Figure 7. The ratio of (efficiency corrected) fitted vs input mean event timescales for our simulated fields as a function of stellar density. The thin and thick lines correspond to 5-parameter (i.e. unconstrained blending) and 4-parameter (i.e. $f_S = 1$) fits, respectively. The dotted/solid/dashed lines denote low/medium/high quality seeing. Note that the 5-parameter fits are very stable and therefore the lines are practically coincident, i.e. all have $\langle t_{E,out} \rangle / \langle t_{E,in} \rangle \approx 1$.

$$\tau_{in} = \frac{1}{TN_{\star,in}} \sum_{i=1}^{N_{events}} 2t_{E,in,i} \sqrt{1 - u_{0,in,i}^2}, \quad (6)$$

where T is the duration of the microlensing experiment, $N_{\star,in}$ is the number of stars in the input field with $I_{in} < 17$ (i.e. before the field has been convolved to ground based seeing), and N_{events} is the total number of microlensing events that have been generated. Note that N_{events} corresponds to the number of events that have been generated, not the number of events that have passed our detection criteria. Since we are interested in the optical depth to bright stars, N_{events} corresponds to the number of events with source magnitude brighter than this cut-off, i.e. $I_{in} < 17$. Also, we only consider events that have peak time within one of the observing seasons, i.e. T does not include the off-season. Therefore our simulations, which are based on three year OGLE-II observations, have $T = 778$ d.

6.1.2 Output optical depth

The input optical depth determined from equation (6) must then be compared to the observed optical depth, τ_{out} , which can be calculated using the conventional equation (e.g. Udalski et al. 1994a),

$$\tau_{out} = \frac{\pi}{2TN_{\star,out}} \sum_{i=1}^{N'_{events}} \frac{t_{E,out,i}}{\epsilon(t_{E,out,i})}, \quad (7)$$

where $N_{\star,out}$ is the number of stars in the *output* field brighter than $I_{out} = 17$ mag, (i.e. the number of bright stars detected by

DoPHOT once the field has been convolved to ground based seeing) and N'_{events} is the total number of microlensing events that have passed the event detection criteria and have well-constrained values for the fitted timescale (see Sections 3 & 5.1.1). N'_{events} only incorporates events with baseline magnitude $I_{out} < 17$ and impact parameter $u_{0,out} < 1.0$. The detection efficiency corresponds to the fraction of events that pass our event detection criteria (see Section 5.1.3). Note that equation (7) is not the only way one can estimate the optical depth; for example, Popowski et al. (2005) advocate a slightly different approach that incorporates the maximum amplification into the detection efficiency.

We estimate two different values of τ : the optical depth estimated under the assumption that bright events are unblended ($\tau_{out,4p}$) and the value estimated when blending is incorporated into the fit ($\tau_{out,5p}$). Each of these τ estimates are based on samples of events created using the respective detection criteria, e.g. for $\tau_{out,4p}$ the detection criteria requires $u_{0,4p} < 1$, while for $\tau_{out,5p}$ the detection criteria requires $u_{0,5p} < 1$. Note that for our blended fits, we only retain events for which the source magnitude is brighter than $I_{S,5p} = 17$ mag, not the total baseline magnitude.

6.2 Results

To assess the reliability of recovering τ for our two methods, we calculate the ratio τ_{out}/τ_{in} for each of our simulated fields. This information is given in Table 1 and is shown in Fig. 8.

In general, the 5-parameter blended fits produce good agreement between τ_{out} and τ_{in} , with an error of less than 20 per cent. Note that the error is less than 10 per cent for all fields except those with lowest quality seeing (i.e. 2.1 arcsec).

This behaviour can be understood as follows. The dominant effect for the 5-parameter fits is the error in the estimation of $N_{\star,\text{out}}$. This value is determined from the number of observed stars with $I_{\text{out}} < 17$ mag, but since a number of stars on the image are blended we find that $N_{\star,\text{out}} > N_{\star,\text{in}}$. Blending can affect the recovery of N_{star} in two ways: firstly, faint stars can be brought into the bright regime by being blended with other faint stars; and secondly, a pair of bright objects can be unresolved and hence be detected as only one object. These are clearly two competing effects, yet the fact that $N_{\star,\text{out}} > N_{\star,\text{in}}$ shows that the former effect is dominant, reflecting the steepness of the luminosity function at the main sequence turn-off. In general we find that $N_{\star,\text{out}}$ overestimates the number of stars by around 10 per cent. However, for the fields with worst seeing the error in $N_{\star,\text{out}}$ can reach as high as 36 per cent, which explains why the error in τ_{out} increases for fields with worse seeing. In theory one could correct for this issue using simulations, although in practise this may be difficult to estimate accurately due to certain observational effects (Sumi et al. 2006).

However, even if we could correct for this issue the problem is not fully resolved. For example, if we use $N_{\star,\text{in}}$ in equation (7) the 5-parameter fit still overestimates the optical depth by around 10 per cent for all fields. This is in part due to minor effects that influence the recovery of τ_{out} , such as incorrectly estimated source magnitude and impact parameter from the model fits. In addition to this, there is an error associated with the fact that to obtain equation (7) from equation (6), one assumes that the impact parameter is uniformly distributed. In practise this is not entirely true since events with impact parameter close to 1 have lower detection efficiency than events with larger magnification (i.e. smaller u_0). This problem can be overcome by using an efficiency that is a function of both t_E and u_0 (e.g. Popowski et al. 2005) or by introducing a correction factor determined from Monte Carlo simulations (such as those presented in this work).

The case for the 4-parameter fits is somewhat less subtle. As has been stated above in Section 5.3, when a sample of bright events are erroneously assumed to exhibit no blending, the fitted timescales are shifted towards smaller values (see Fig. 5 and Table 1). However, the effect on the optical depth is counterbalanced by the increase in the number of observed events, i.e. a number of events with source star magnitudes fainter than the cut-off are included in the sample due to blending (see, for example, Alcock et al. 1997b). For example, in our reference field we find that 22 per cent of bright events are actually caused by fainter sources with $I_{S,\text{in}} > 17$. In our extreme case of lowest quality seeing and highest density this fraction rises to 47 per cent. Owing to the cancellation of these two effects, from Table 1 we see that the error in the unblended optical depth is less than 7 per cent for all of our simulated fields, even for those with highest stellar density or worst quality seeing. In most cases the recovered optical depth is slightly lower than the input value, but such an error can be considered negligible compared to the statistical errors that will be present in any current real-life experiment. It should also be noted that there are a number of additional factors that affect the final optical depth, such as the fact that many events with $u_{0,\text{in}} < 1$ have $u_{0,4p} > 1$ after fitting with a model assuming no blending (see Fig. 5). As was discussed in Section 5.3, there is the issue of bright source stars being blended with nearby faint stars, but we have found this to have only limited influence. The problem described above of incorrectly determining

$N_{\star,\text{out}}$ also affects the 4-parameter fits, although in this case it is not the dominant factor. However, this will still bias the optical depth towards smaller values.

7 CENTROID MOTION AND CENTROID-SOURCE OFFSET FOR BLENDED EVENTS

As has been shown in Section 2.2, it is possible to identify blended microlensing events through their centroid motion, or equivalently the offset between the baseline centroid and the lensed source.

In Fig. 9 we show the distribution of the offset between the baseline centroid and the lensed source for our simulated fields,

$$\Delta r = \left| \frac{(\mathbf{r}_{\text{source}} - \mathbf{r}_{\text{blend}})F_{\text{blend}}}{F_{\text{blend}} + F_{\text{source}}} \right|, \quad (8)$$

where $\mathbf{r}_{\text{blend}}$ and $\mathbf{r}_{\text{source}}$ denote the location of the blend and source centroid, respectively, and F_{blend} and F_{source} denote the blend and source flux, respectively. From Fig. 9 it is clear that for almost all fields a significant fraction of events exhibit noticeable offsets of more than 0.2 arcsec. Although Δr is reduced for the bright samples of stars, there is still greater than 10 per cent with $\Delta r > 0.2$ arcsec. The amount of offset is particularly severe for the fields with low quality seeing; for example, for field s1d2, which has a seeing of 2.1 arcsec, more than 80 per cent of events have $\Delta r > 0.2$ arcsec, even for the bright sample.

However, one must interpret this figure with caution because one cannot simply deduce that all of the events with large offset are heavily blended. For fields with low quality seeing (2.1 arcsec), as many as 50 per cent of bright, *unblended* ($0.7 < f_S < 1.3$) events have $\Delta r > 0.2$ arcsec. Fortunately this problem is reduced for fields with better quality seeing, such as our reference field (seeing 1.05 arcsec); of the bright events in this field with $\Delta r > 0.2$ arcsec, only 8 per cent show no significant blending (i.e. $f_S > 0.5$). However, the problem remains for low quality seeing, even in the sample of bright stars. Therefore, it is apparent that if one wishes to use such information to quantify the level of blending, then this must be used with caution. In particular, it is unlikely that any meaningful results can be obtained for cases of low quality seeing (e.g. 2.1 arcsec).

It is also possible to calculate the maximum centroid motion ($\Delta r'$) that would be observed for the events in our simulations. Given that the location of the centroid can be expressed as,

$$\mathbf{r}(t) = \frac{\mathbf{r}_{\text{blend}}F_{\text{blend}} + \mathbf{r}_{\text{source}}F_{\text{source}}A(t)}{F_{\text{blend}} + F_{\text{source}}A(t)}, \quad (9)$$

where $A(t)$ denotes the magnification at time t . Given this formula it is trivial to derive the expression for the maximum centroid motion,

$$\Delta r' = \left| \frac{F_{\text{blend}}F_{\text{source}}(A_{\text{peak}} - 1)(\mathbf{r}_{\text{source}} - \mathbf{r}_{\text{blend}})}{(F_{\text{blend}} + F_{\text{source}}A_{\text{peak}})(F_{\text{blend}} + F_{\text{source}})} \right|, \quad (10)$$

where A_{peak} is the maximum magnification. This equation can equivalently be expressed in terms of the centroid-source offset (Δr , given in equation 8),

$$\Delta r' = \Delta r \frac{F_{\text{source}}(A_{\text{peak}} - 1)}{F_{\text{blend}} + A_{\text{peak}}F_{\text{source}}}, \quad (11)$$

Clearly this maximum centroid motion corresponds to the difference between the location of the centroid at baseline and at peak magnification, and hence is an upper limit to the observed motion since the event may not be observed exactly at peak magnification.

The cumulative distribution for $\Delta r'$ is shown in Fig. 10. As expected, this figure shows similar behaviour to the corresponding plot of baseline centroid-source offsets, although the offsets are

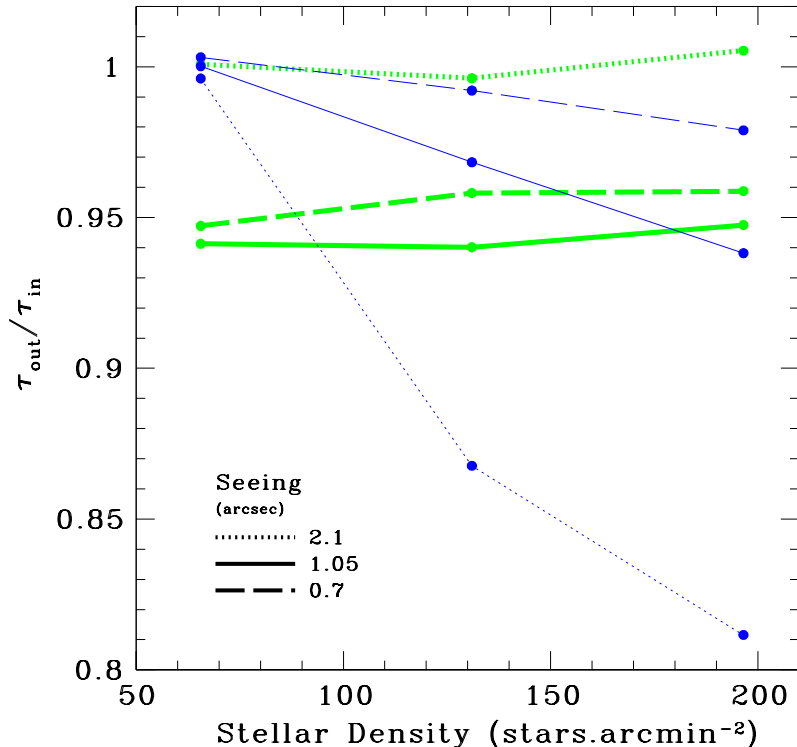


Figure 8. The ratio between the input and output optical depth for 4-parameter (i.e. $f_S = 1$; thick) and 5-parameter (i.e. unconstrained blending; thin) fits for our simulated fields. The dotted/solid/dashed lines denote low/medium/high quality seeing.

somewhat smaller. For example, for our reference field (medium seeing and density) 30 per cent of all events and less than 10 per cent of bright events have $\Delta r' > 0.2$ arcsec.

8 DISCUSSION

This paper has provided a detailed investigation into the nature of blending in gravitational microlensing experiments towards the Galactic bulge. As we have discussed in Section 2, it is clear that for some bright events blending can be significant. Our simulations also support this claim. In Section 4 we showed the true underlying blending distributions for our simulated fields, all of which exhibit blending to varying degrees. We can conclude that the dominant source of blending is from lensing of faint source stars, rather than lensing of bright source stars blended with nearby fainter stars.

However, the results from our simulations (Sections 3 – 6) indicate that this issue may not be as troublesome as one might fear. Although the event timescale is unquestionably affected, the optical depth determinations in most cases are robust across a range of seeing and density. The fact that the optical depth is reliably recovered even from a sample of blended events is particularly important; however, this reliable recovery appears to rely on a coincidental cancelling out of two factors (an underestimation in the timescale and a corresponding overestimation of the number of events). This finding is not new, but to discover that it holds for various values of seeing and density in our simulation is reassuring. Clearly we do not advocate that our results should be applied directly to any real

experiments, since the details will depend on the individual experimental set-up and event detection criteria.

The results in Section 5 are of slightly greater concern in relation to the recovery of the event timescale. If we (erroneously) assume that our bright events are unblended then this clearly results in an underprediction of the event timescale of between 10 and 40 per cent. It has been argued that the extent of this problem can be reduced if one only deals with high amplification events. For example, the recent papers of Popowski et al. (2005) and Hamadache et al. (2006) advocate only using events with amplification greater than 1.5 and 1.6, respectively. If we apply this restriction to our simulations then the level of discrepancy between the fitted and input timescale is reduced slightly; for example, if we apply the restriction that the $A > 1.6$ for our reference field we find that the ratio between the fitted and input t_E becomes 0.81, which is only a slight improvement compared to the ratio 0.77 that was found for events with $A > 1$. Although this does improve the situation, it is far from resolving the problem. This underprediction could help to explain the discrepancy in $\langle t_E \rangle$ between Popowski et al. (2005; $\langle t_E \rangle = 15 \pm 15$ d) and Sumi et al. (2006; $\langle t_E \rangle = 28.1 \pm 4.3$ d), since the former work assumes that their bright events are unblended while the latter work incorporates blending into their model fitting. However, there are large errors on $\langle t_E \rangle$ for Popowski et al. (2005) and hence the discrepancy is only very weak. It is also interesting to note that another recent clump giant survey that assumes no blending (Hamadache et al. 2006; $\langle t_E \rangle = 28.3 \pm 2.8$ d) finds a value that is in good agreement with Sumi et al. (2006), although owing to their

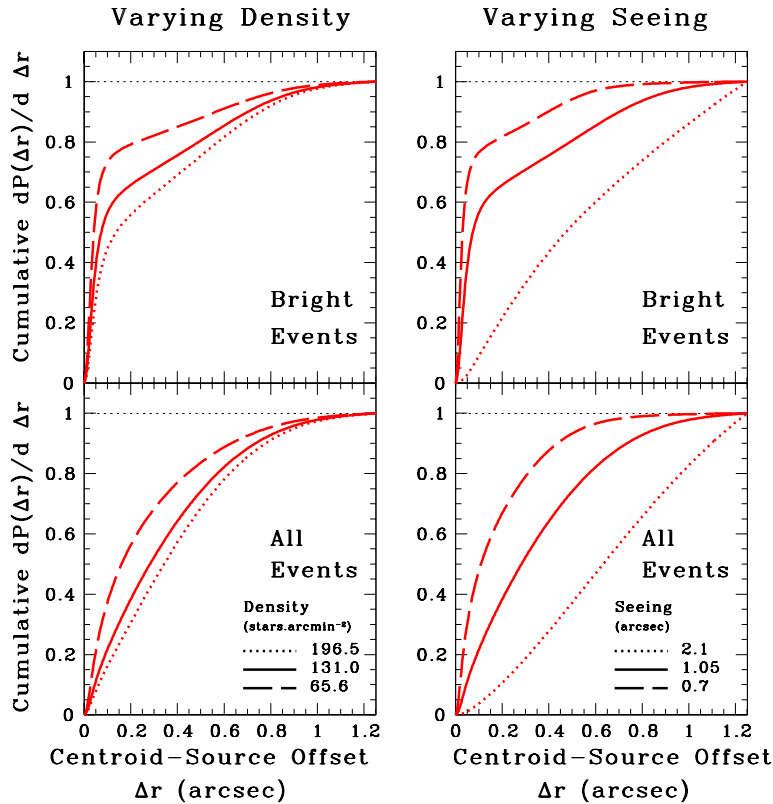


Figure 9. The distributions for the offset between the baseline centroid and the lensed source for microlensing events in our simulated fields. The upper panels show the distribution for a bright subset of events ($I_{\text{out}} < 17$), such as red clump giants, and the lower panels show the distribution for all events ($I_{\text{out}} < 19$). The left panels show fields with differing stellar density (dotted/solid/dashed correspond to high/medium/low density) while the right panel shows fields with differing values for the seeing (dotted/solid/dashed corresponds to low/medium/high quality seeing). Note that in our simulations one pixel corresponds to 0.417 arcsec.

larger spatial coverage one might expect them to find a larger $\langle t_E \rangle$ (e.g., Wood & Mao 2005).

An aspect of blending that has been ignored in this work is that of colour. Clearly if the colour of the blend and the source are different, then the microlensing amplification will be chromatic (e.g., Kamionkowski 1995; Buchalter, Kamionkowski, & Rich 1996). The strategy for the OGLE experiment has been to take practically all observations in the I -band, with only very limited sampling in the V -band for determining baseline colour information. However, EROS and MACHO both have colour information, although in their optical depth papers (Popowski et al. 2005, Hamadache et al. 2006) colour information was not used to discriminate individual blended events (although the former work did note that the colour variation of their sample was consistent with expectations for a sample of unblended events).

Although the work presented here has dealt with the issues relating to blending from stars that are coincidentally located close to a microlensed source, there is an additional factor that we have not considered, namely the luminosity of the lens. By definition every microlensed source must be coincident with a lens star. Various works have attempted to address how this fact affects the amount of blending and the recovery of parameters from a theoretical standpoint (e.g., Kamionkowski 1995; Nemiroff 1997; Han 1998). In addition, for one event towards the LMC (Alcock et al. 2001b) and at least one event towards the Galactic bulge (Kozłowski et al., in

preparation) the lens and source have actually been resolved, implying that for these events the lens contributes a finite amount of flux to the total blended light. If more events can be found for which the lens and source are resolvable, it will provide a promising way to empirically quantify the effect of lens blending. Since the Monte Carlo analysis presented here (Sections 3 – 6) has not incorporated this lens flux, our work can be considered to underestimate the effect of blending.

One obvious deficiency in this work (and all other similar work) is the lack of available deep luminosity functions for the different lines of sight towards the bulge. Deep HST luminosity functions, such as the Holtzman et al. (1998) one, would be very valuable if they were available across different bulge fields. A project to tackle this issue is currently underway (Kozłowski et al., in preparation).

Data from projects such as OGLE-II can (and have) been used for additional purposes not directly related to microlensing, such as producing extinction maps (e.g. Sumi 2004) and constraining the parameters of the Galactic bar through red clump giant number counts (e.g. Rattenbury et al. 2007). These studies will also be affected by the problems of stellar crowding. For example, any work that wishes to determine the centre of the red clump giant region will find it systematically shifted towards brighter magnitudes due to blending. From our simulations we can estimate this effect; by fitting our observed luminosity function with a power-law plus

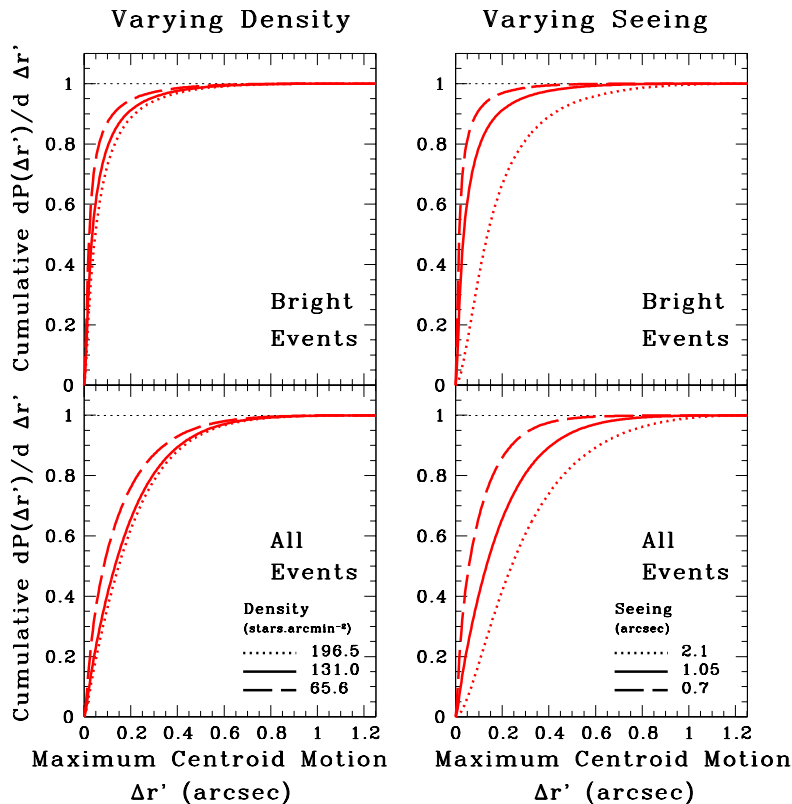


Figure 10. As Fig. 9 except this shows the centroid motion for microlensing events in our simulated fields. The centroid motion corresponds to the motion that would be observed if the event were observed at the peak magnification (see Section 7).

Gaussian (where the Gaussian represents the red clump stars; see, for example, equation 4 of Sumi 2004) one can easily determine the shift. For our reference field we find that the Gaussian is centred on an I-band magnitude of 16.062 ± 0.004 and 15.918 ± 0.005 for the input (i.e. HST) and output (i.e. after convolving to ground-based seeing) luminosity functions, respectively, i.e. a shift of 0.144 mag. Such a shift can have an important effect in applications such as those mentioned above. However, for the issue of extinction, one is often more interested in the colour of the centre of the red clump region. Since we do not have any colour information in our simulations we cannot address this point, but from Fig. 2 it can be seen that if the blend is caused by a star that is less than ~ 2 magnitudes fainter than the red clump region, then there will be a systematic blueward shift.

In conclusion, we confirm that blending has only a limited impact on the recovery of optical depth for the current generation of microlensing experiments. In Section 6 we have shown that the recovered optical depth is probably reliable to within ~ 10 per cent. However, it is now becoming clear that with the improved accuracy of future experiments, microlensing surveys will not be able to hide from the issue of blending. Such work must undertake a detailed and thorough treatment of this effect otherwise their results could be subject to significant bias.

ACKNOWLEDGMENTS

The authors are indebted to the referee, Andy Gould, for providing useful suggestions and comments. We also wish to thank Dave Bennett for raising the issue of blending related bias in the estimation of extinction. MCS acknowledges financial support by PPARC and the Netherlands Organisation for Scientific Research (NWO). PW was supported by the Oppenheimer Fellowship at LANL. TS acknowledges financial support from the JSPS and also benefited from the financial help of the visitor's grant at Jodrell Bank. This work was partially supported by the European Community's Sixth Framework Marie Curie Research Training Network Programme, Contract No. MRTN-CT-2004-505183 'ANGLES'.

REFERENCES

- Alard C., Mao S., Guibert J. 1995, *A&A*, 300, L17
- Albrow M.D. et al., 1999, *ApJ*, 522, 1022
- Alcock C. et al., 1997a, *ApJ*, 479, 119
- Alcock C. et al., 1997b, *ApJ*, 486, 697
- Alcock C. et al., 2000, *ApJ*, 541, 734
- Alcock C. et al., 2001a, *ApJ*, 552, 582
- Alcock C. et al., 2001b, *Nature*, 414, 617
- Afonso C. et al., 2003, *A&A*, 404, 145
- Binney J., Bissantz N., Gerhard O., 2000, *ApJ*, 537, L99
- Bond I.A. et al, 2001, *MNRAS*, 327, 868
- Buchalter A., Kamionkowski M., Rich R.M., 1996, *ApJ*, 469, 676
- Dominik M., 1999, *A&A*, 341, 943

- Evans N.W., 2003, in Valls-Gabaud D., Kneib J.-P., eds, *Gravitational Lensing: A Unique Tool For Cosmology* (astro-ph/0304252)
- Evans N.W., Belokurov V., 2002, *ApJ*, 567, L119
- Gaudi S., Han, C. 2004, *ApJ*, 611, 528
- Gould A., 1992, *ApJ*, 392, 442
- Gould A., 1995, *ApJ*, 447, 491
- Gould A., An J., 2002, *ApJ*, 565, 1381
- Goldberg D.M., 1998, *ApJ*, 498, 156
- Goldberg D.M., Woźniak P.R., 1998, *AcA*, 48, 19
- Hamadache C., 2006, *A&A*, 454, 185
- Han C., 1997, *ApJ*, 490, 51
- Han C., 1998, *ApJ*, 500 569
- Han C., 1999, *MNRAS*, 309, 373
- Han C., 2000, *JKAS*, 33, 89
- Han C., Gould A., 2003, *ApJ*, 592, 172
- Holtzman J.A., Watson A.M., Baum W.A., Grillmair C.J., Groth E.J., Light R.M., Lynds R., O'Neil E.J., 1998, *AJ*, 115, 1946
- James F., 1994, *Minuit Reference Manual*, CERN Program Library
- Jaroszyński M. 2002, *Acta Astronomica*, 52, 39
- Jaroszyński M. et al., 2004, *AcA*, 54, 103
- Jiang G, 2004, *ApJ*, 617, 1307
- Kamionkowski M., 1995, *ApJ*, 442, L9
- Kim S., 2004, MSc thesis, Univ. of Manchester
- Mao S., Di Stefano R. 1995, *ApJ*, 440, 22
- Mao S., 1999, in Brainerd T.G., Kochanek C.S., eds., *Gravitational Lensing: Recent Progress and Future Goals* (astro-ph/9909302)
- Nemiroff R.J., 1997, *ApJ*, 486, 693
- Paczyński B., 1996, *ARAA*, 34, 419
- Palanque-Delabrouille N. et al., 1998, *A&A*, 332, 1
- Park B.-G. et al., 2004, *ApJ*, 609, 166
- Poindexter S., Afonso C., Bennett D.P., Glicenstein J-F., Gould A., Szymański M.K., Udalski A., 2005, *ApJ*, 633, 914
- Popowski P. et al., 2005, *ApJ*, 631, 879
- Rattenbury N.J., Mao S., Sumi T., Smith M.C., 2007, *MNRAS*, 378 1064
- Schechter P.L., Mateo M., Saha A., 1993, *PASP*, 105, 1342
- Smith M.C. et al., 2002, *MNRAS*, 336, 670
- Smith M.C., Belokurov V., Evans N.W., Mao S., An, J.H., 2005, 361, 128
- Sumi T., 2004, *MNRAS*, 349, 193
- Sumi T. et al., 2003, *ApJ*, 591, 204
- Sumi T. et al., 2006, *ApJ*, 636, 240
- Udalski A., 2003, *Acta Astron.*, 53, 291
- Udalski A. et al., 1994a, *Acta Astron.*, 44, 165
- Udalski A., Szymański M., Mao S., Di Stefano R. I., Kałużny J., Kubiak M., Mateo M., Krzemiński W. 1994b, *ApJ*, 436, L103
- Udalski A., Żebruń K., Szymański M., Kubiak M., Pietrzyński G., Soszyński I., Woźniak P., 2000, *Acta Astron.*, 50, 1
- Smith M.C., Belokurov V., Evans N.W., Mao S., An, J.H., 2005, *MNRAS*, 361, 128
- Witt H.J., Mao S., 1995, *ApJ*, 447, L105
- Wood A., Mao S., 2005, *MNRAS*, 362, 945
- Woźniak P., 2000, *AcA*, 50, 421
- Woźniak P., Paczyński B., 1997, *ApJ*, 487, 55
- Woźniak P.R., Udalski A., Szymański M., Kubiak M., Pietrzyński G., Soszyński I., Żebruń K., 2001, *Acta Astron.*, 51, 175
- Woźniak P.R., Udalski A., Szymański M., Kubiak M., Pietrzyński G., Soszyński I., Żebruń K., 2002, *Acta Astron.*, 52, 129
- Zhao H.S., Mao S., 1996, *MNRAS*, 283, 1197

Seeing (arcsec)	Input stellar density (stars.arcmin ⁻²)	“Observed” stellar density (stars.arcmin ⁻²)	Stars per “seeing disc” (stars)	Magnitude cut	$f_S < 0.2$ (%)	$f_S < 0.5$ (%)	$0.8 < f_S < 1.2$ (%)	$f_S > 1.5$ (%)	$\langle t_{E,4p} \rangle / \langle t_{E,in} \rangle$	$\langle t_{E,5p} \rangle / \langle t_{E,in} \rangle$	$\tau_{out,4p} / \tau_{in}$	$\tau_{out,5p} / \tau_{in}$
2.1	66.7	74.1	231.0	$I_{out} < 19$	30.5	58.0	18.7	3.7	-	-	-	-
				$I_{out} < 17$	32.1	38.2	41.5	7.1	0.830	1.011	1.001	0.996
2.1	133.1	167.6	461.0	$I_{out} < 19$	45.5	70.8	11.4	3.6	-	-	-	-
				$I_{out} < 17$	47.6	57.5	21.7	6.6	0.699	1.007	0.996	0.868
2.1	198.6	263.5	687.9	$I_{out} < 19$	54.8	76.4	9.3	2.8	-	-	-	-
				$I_{out} < 17$	56.3	68.0	15.2	4.3	0.603	1.008	1.005	0.812
1.05	66.7	72.2	57.8	$I_{out} < 19$	19.3	38.9	38.9	0.8	-	-	-	-
				$I_{out} < 17$	19.4	21.8	72.8	0.8	0.871	1.014	0.941	1.000
1.05	133.1	149.0	115.3	$I_{out} < 19$	29.9	56.6	22.8	0.8	-	-	-	-
				$I_{out} < 17$	31.7	35.9	55.1	0.8	0.773	1.007	0.940	0.968
1.05	198.6	229.2	172.0	$I_{out} < 19$	37.4	65.5	16.7	0.7	-	-	-	-
				$I_{out} < 17$	40.2	46.1	42.3	0.8	0.711	1.010	0.947	0.938
0.7	66.7	72.3	25.7	$I_{out} < 19$	13.2	27.0	53.4	0.9	-	-	-	-
				$I_{out} < 17$	12.1	15.2	74.7	2.4	0.915	1.009	0.947	1.003
0.7	133.1	146.2	51.2	$I_{out} < 19$	19.3	39.4	38.0	0.8	-	-	-	-
				$I_{out} < 17$	19.2	22.0	69.9	2.1	0.880	1.014	0.958	0.992
0.7	198.6	220.4	76.4	$I_{out} < 19$	25.1	50.0	27.8	0.7	-	-	-	-
				$I_{out} < 17$	25.8	29.3	61.7	1.7	0.827	1.011	0.959	0.979

Table 1. Quantitative comparison of all nine simulated fields. The first four columns describe the setup of our simulated fields, while the remaining columns show the fraction of blended events (columns 6–9), the ratio between the input and fitted t_E (columns 10 & 11) and the ratio between the input and fitted τ (columns 12 & 13). The subscript 4p indicates a four-parameter fit (i.e. $f_S = 1$), while the subscript 5p indicates a five-parameter fit with unconstrained blending (see Section 5.1.2). The fractions of blended events correspond to the input blending distributions, not the fitted distributions. Note that $f_S > 1$ corresponds to negatively blended events. Stellar densities are quoted for stars with $I < 17$.

	$f_S < 0.2$ (%)	$f_S < 0.5$ (%)	$f_S > 1.0$ (%)	$f_S > 1.5$ (%)
$13.5 < I_{\text{out}} < 14.5$	14.4	15.8	15.6	2.3
$14.5 < I_{\text{out}} < 15.5$	25.2	28.1	9.3	0.8
$15.5 < I_{\text{out}} < 16.5$	33.0	36.0	8.4	0.5
$16.5 < I_{\text{out}} < 17.5$	37.6	49.5	7.6	0.9
$17.5 < I_{\text{out}} < 18.5$	31.3	62.8	5.5	0.6
$18.5 < I_{\text{out}} < 19.5$	21.3	58.6	8.1	1.3

Table 2. Percentage of blended events as a function of I_{out} for our field with medium quality seeing and medium density. These percentages correspond to the input blending distributions ($f_{S,\text{in}}$), not the fitted distributions.